Journal of Porphyrins and Phthalocyanines
J. Porphyrins Phthalocyanines 2017; **21**: 1–9
DOI: 10.1142/S1088424617500390

Published at http://www.worldscinet.com/jpp/

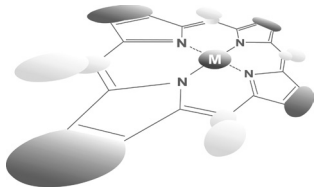

Effect of functional groups on sensitization of dye-sensitized solar cells (DSSCs) using free base porphyrins

Nivedita Chaudhri,[a] Nipun Sawhney,[b] Bijjam Madhusudhan,[a] Anubhav Raghav,[b] Muniappan Sankar[a*◊] and Soumitra Satapathi[b*]

[a]*Department of Chemistry, Indian Institute of Technology Roorkee, Roorkee-247667, India.*
[b]*Department of Physics, Indian Institute of Technology Roorkee, Roorkee-247667, India.*

Received date: 8 February 2017
Accepted date: 27 April, 2017

ABSTRACT: Dye-sensitized solar cells (DSSCs) were fabricated with six *meso*-substituted A_3B and A_4 free base porphyrin dyes having different functional groups, as sensitizers. The two step synthesis and the effect of different functional groups and their positions on the photosensitization properties of these porphyrin dyes are reported. The highest power conversion efficiencies (η) of 3.26%, 2.94% and 2.84% were achieved for the DSSC fabricated using 5,10,15-tris(4′-pyridyl)-20-(4′-carboxyphenyl)porphyrin (H_2TriPyMCPP), 5,10,15,20-tetrakis(4′-aminophenyl)porphyrin (H_2TAPP) and 5-(4′-pyridyl)-10,15,20-tris(4′-carboxyphenyl)porphyrin (H_2MPyTriCPP) dyes, respectively. The electron donating amino group is shown to enhance the power conversion efficiency while pyridyl appended porphyrin sensitizers are shown to be superior sensitizers as compared to carboxyphenylporphyrins. The investigation of effect of functional group and position of functional group of porphyrin dye on DSSC can serve as an important tool to guide further selection and synthesis of potential candidates as sensitizers.

KEYWORDS: porphyrins, photosensitizers, dye-sensitized solar cell, power conversion efficiency.

INTRODUCTION

Dye-sensitized solar cells (DSSCs) as discovered by Grätzel in 1991, have attracted tremendous research interest due to their low cost, ease of fabrication, short energy payback time, low sensitivity to temperature variation, versatility, and environment friendly fabrication [1, 2]. A DSSC is composed of a nanocrystalline porous layer of titanium dioxide (TiO_2) coated photoanode, a monolayer of dye molecules that absorbs sunlight, an electrolyte for dye regeneration and a cathode. The anode and cathode form a sandwich structure, while the photosensitizer (dye) plays a crucial role by absorbing photons from sunlight. A significant amount of research has been undertaken to modify the structure and composition of dye molecules in order to enhance the absorption of sunlight in order to increase the power conversion efficiency (PCE) of these solar cells [3]. Initially, Ru(II) based complexes had received particular interest as a photosensitizers because of their long-term chemical stability, longer exciton lifetime and broad absorption spectra due to metal-to-ligand charge transfer [4]. Polypyridyl Ru(II)-based dyes have been utilized to achieve the maximum PCE of 11.5% [5]. However, scarcity of noble metals, lower molar extinction coefficient, high cost and environmental issue of Ru(II) dyes limit their large scale commercialization [6]. In this regard, a large number of steps have been taken to develop efficient sensitizers that exhibit high molar absorption coefficients with high suitability for large scale applications. As feasible alternatives, metal free organic dyes with D-π-A or push–pull architecture have been used to improve short circuit current density JSC [7]. To overcome the high cost of ruthenium complexes, metal free organic dyes have been extensively explored in the recent years.

Organic dyes including porphyrins, coumarins, perylenes, phthalocyanines, carbazoles, triarylamine, perylene, cyanine, fluorene, merocyanine and hemicyanine

◊ SPP member in good standing.
*Correspondence to: Muniappan Sankar, email: sankafcy@iitr.ac.in, tel: +91 1332-284753,, Saumitra Satapathi, email: ssphf.fph@iitr.ac.in

derivatives *etc*. have been utilized extensively [8, 9]. Among these, porphyrins have attracted considerable attention as light-harvesting antennae for DSSCs due to their unique photophysical and electrochemical redox properties, thermal and chemical stability, and high efficiency in absorbing solar energy in the visible region due to their high molar extinction coefficients making them suitable candidates for the development of panchromatic sensitizers [10, 11]. Metalloporphyrins, especially Zn(II) porphyrins have been commonly used in DSSCs to attain the high PCE value and have gained tremendous research interest in recent years [11a, 12, 13]. Despite their high efficiencies in DSSCs, the effect of different functional groups on light harvesting properties of porphyrin dyes remains relatively unexplored [14]. Herein, we have synthesized highly symmetrical A_4 and unsymmetrical A_3B type free base porphyrins (Chart 1). Further, we have examined photophysical and photovoltaic properties of these porphyrin dyes to provide a detailed explanation of the effect of functional groups on their sensitization properties in DSSCs.

EXPERIMENTAL SECTION

Chemicals and Materials

Pyrrole, KOH and Na_2SO_4 were purchased from HiMedia, India and used as received. Propionic acid was purchased from SDFCL and used without further purification. All aromatic aldehydes used in the presenting work were purchased from Alfa Aesar and used as received. All the solvents employed in the electronic spectral and electrochemical studies were of analytical grade and distilled or dried before use. $TBAPF_6$ for cyclic voltammetric studies was purchased from Alfa Aesar and twice recrystallized from ethanol and dried for two days under vacuum at 60 °C. FTO coated Glass, I^-/I_3^- electrolytes and Pt Paste were purchased from Dyesol, Australia. Titanium(IV) isopropoxide, spectroscopic grade ethanol and tetrahydrofuran were purchased from HiMedia, India and used without further purification.

Instrumentation and Methods

UV-visible absorption spectra were recorded with a pair of quartz cells of 3 ml volume and 10 mm path length in distilled CH_2Cl_2 using an Agilent Cary 100 spectrophotometer. The fluorescence emission spectra were recorded on a Hitachi F-4600 spectrofluorometer using a quartz cell of 10 mm path length and 3 ml volume. ^{1}H NMR spectra were recorded on JEOL ECX 400 MHz spectrometers using $CDCl_3$ as a solvent containing 0.03% TMS (v/v). MALDI-TOF-MS spectra were measured using a BrukerUltrafleXtreme-TN MALDI-TOF/TOF spectrometer using HABA as a matrix and DFT studies were carried out using B3LYP functional with 6-31 G basis set with the Gaussian 03 software package. The HOMO and LUMO levels were obtained from ground state redox potentials and the difference of the potentials for the NHE (Uredox) an electron in vacuum (E, Fredox).

Scanning Electron Microscopy images of electrodes were taken after sputtering the surface with gold using Scanning Electron Microscope (JEOL JEM2010) operated at 15 kV and magnification of 2000X. All cells corresponding were tested under 350 W/m^2 illuminations using artificial sunlight using Zahner's CIMPS-QE/IPCE system and Newport CIMPS-QE/IPCE system respectively.

Fabrication of DSSCs

FTO slides were successively cleaned in distilled water, ethanol and acetone for cycles of 30 min each respectively. Synthesis of nano-crystalline TiO_2 was done through hydrolysis of titanium(IV) isopropoxide [15]. Titanium(IV) isopropoxide was mixed with ethanol, and the mixture was stirred at 800 rpm for 30 min on a

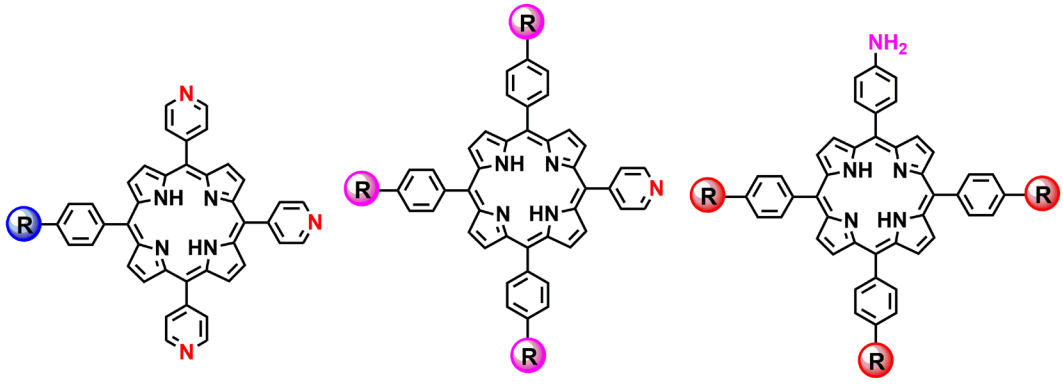

Chart 1. Molecular structures of synthesized free base porphyrins

magnetic stirrer. This was followed by ultrasonicated for 30 min and then 24 mL distilled water was added at pace of nearly 0.5 mL/min for 48 min using a micropipette. The mixture was then heated to 353 K under reduced pressure to remove the solvent. It was then further dried in an oven at 393 K for a few hours to obtain dry TiO_2 powder. TiO_2 powder was then calcined in a muffle furnace at 673 K to produce anatase TiO_2 nanoparticles. TiO_2 slurry was then obtained by slowly adding acetic acid solution (pH = 3). The slurry was ultrasonicated for 30 min, and was placed on a magnetic stirrer at 1200 rpm for 30 min. Ultrasonication and stirring was repeated four times to get consistent viscous slurry of TiO_2.

The prepared TiO_2 slurry was then doctor bladed on FTO glass slide using doctor tape (30 μm) on one side and sintered at an optimized temperature of 823 K to prepare mesoporous nanocrystalline TiO_2 photo anodes. The photo anodes were dipped in the respective dye solutions for 12 h for complete dye loading. A pt counter electrode was fabricated through drop casting and sintering [16]. The electrodes and counter electrodes were used to make sandwiched devices with active cell area of 0.15 cm^2.

Synthesis and Characterization

The above mentioned A_3B and A_4 type porphyrins (Chart 1) have been synthesized in two steps using modified literature methods [17–19] *via* simple condensation reaction between pyrrole and various substituted benzaldehydes in propionic acid. The detailed synthetic procedures are given in the experimental section. Ester porphyrins were subjected to alkaline hydrolysis to obtain the corresponding carboxyphenylporphyrins. Scheme 1 shows the synthetic route for the preparation of 2a and 2b whereas, Scheme S1 represents the synthetic route for the preparation of 1a and 1b. The nitroporphyrins were subjected to reduction using $SnCl_2$/HCl as shown in Scheme S2 in supporting information.

The synthesized porphyrins were characterized by various spectroscopic techniques *viz*. UV-Vis, fluorescence, ^{1}H NMR and mass spectrometry. The structural information of these dyes has been explained using DFT calculations.

Synthetic Procedures

5-(4′-carbomethoxyphenyl)-10,15,20-tris(4′-pyridyl) porphyrin (H_2TriPyMCMPP) and 5-(4′-carboxyphenyl)-10,15,20-tris(4′-pyridyl)porphyrin (H_2TriPyMCPP) were synthesized according to the reported procedure and the spectroscopic data exactly matches with reported procedure [17].

Synthesis of 5-(4′-pyridyl)-10,15,20-tri(4′-carboxyphenyl) porphyrin (H_2MPyTriCPP)

(H_2MPyTriCPP) was synthesized by two step procedure as reported in literature [18]. First step is simple condensation of a 3:1 mixture of pyridine-4-carbaldehyde and 4-methoxy carbonylbenzaldehyde with pyrrole in propionic acid using Adler's Method which gives 5-(4′-pyridyl)10,15,20-tris(4′-methoxycarbonylphenyl) porphyrin (H_2MPyTriCMPP). The second step is alkaline hydrolysis of H_2MPyTriCMPP, where 0.1 g (0.126 mmol) of H_2MPyTriCMPP was dissolved in 25 ml of THF. To this, 0.35g (6.2 mmol) of KOH in 0.4 ml of water was added and heated at 75 °C for 16 h. The course of the reaction was monitored by TLC and the crude porphyrin was treated with a 2N HCl solution, which yielded a green-colored precipitate that was filtered and washed with water several times and dried under vacuum. The protonated porphyrin was neutralized by triethylamine and solvent was removed by rotatory evaporator. The yield of the product was found to be 72% (68 mg, 0.091 mmol). Spectroscopic data are in accordance with the reported literature.

^{1}H NMR (DMSO-d_6), δ (ppm) : 13.30 (s, 3H, -COOH), 9.07 (d, *J* = 4 Hz, 2H, Py-*meso-m*-phenyl), 8.91 (s, 6H, *β*-pyrrole), 8.80 (s, 2H, *β*-pyrrole), 8.36–8.28 (*m*, 12H, *meso-m*, *p*-phenyl), 8.24 (d, J = 4 Hz, 2H, Py-*meso-o*-phenyl), -2.97 (s, 2H). UV/Vis in CH_2Cl_2: λmax [nm] 416, 513, 547, 589, 648. MALDI-TOF-MS (m/z): found 748.06, calculated 747.77 for $C_{46}H_{29}N_5O_6$.

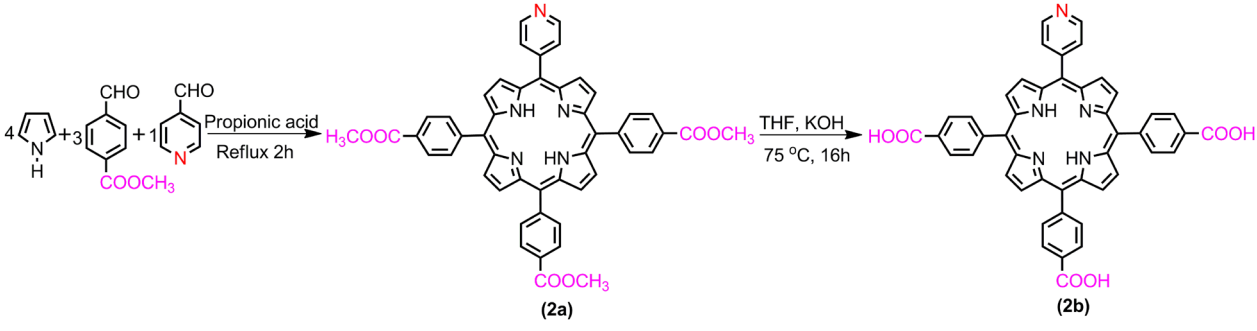

Scheme 1. Synthetic route for the preparation of H_2MPyTriCMPP **(2a)** and H_2MPyTriCPP **(2b)**.

Synthesis of 5,10,15,20-tetrakis(4′-aminophenyl) porphyrin (H_2TAPP)

Synthesis of H_2TAPP was started with the preparation of 5,10,15,20-tetrakis(4′-nitrophenyl)porphyrin, H_2TNPP. H_2TNPP was synthesized by condensing pyrrole with 4-nitrobenzaldehyde in propionic acid as reported in the literature [19]. H_2TAPP was prepared using modified reported procedure [19]. A 100 ml two neck RB was charged with H_2TNPP (0.1 g, 1.26 mmol) in 15 ml of conc. HCl and then purged with argon for 1 h at 0 °C. To this, 24 equivalents of $SnCl_2 \cdot 2H_2O$ in 10 ml of concentrated HCl was added under Argon atmosphere and then the reaction mixture was heated for 20 h at 65 °C. At the end of this period, the reaction mixture was cooled to room temperature and neutralized using 25% NH_4OH solution. The porphyrin precipitate was filtered using G-4 crucible and washed with 20% NaOH solution followed by extraction with $CHCl_3$. The yield of the product was found to be 74% (63 mg, 0.093 mmol). The crude porphyrin was purified by column chromatography on basic alumina using $CHCl_3$/acetone as eluent.

^{1}H NMR in $CDCl_3$, δ (ppm) 8.8 (s, 8H, *β*-pyrrole-H), 7.9 (d, 8H, *meso-o*-phenyl H), 7.0 (d, 8H, *meso-m*-phenyl-H), 4.02 (s, 8H, NH_2), -2.9 (s, 2H, NH). UV/Vis in CH_2Cl_2: λ max [nm] 427, 522, 564, 596, 654. ESI-MS (m/z): 675.3002 [M]+ (calcd., 675.300) for $C_{44}H_{34}N_8$.

Synthesis of 5,10,15-triphenyl-20-(4′-aminophenyl) porphyrin (H_2TriPMAPP)

The free base 5,10,15-triphenyl-20-(4′-aminophenyl) porphyrin (H_2TriPMAPP) was synthesized by a two-step procedure. The first step is the synthesis of 5,10,15-triphenyl-20-(4′-nitrophenyl)porphyrin (H_2TriPMNPP) by Adler's method. This involves the condensation of 3:1 mixture of benzaldehyde and 4-nitrobenzaldehyde with pyrrole in propionic acid. The desired porphyrin was obtained by column chromatography using $CHCl_3$/acetone mixture as second fraction with 12% yield. Thus, the isolated 5,10,15-triphenyl-20-(4′-nitrophenyl)porphyrin was converted into amine porphyrin by reduction with tin chloride dihydrate. H_2TriPMNPP (0.4 g, 0.606 mmol) was dissolved in con. HCl and then purged with argon for 45 min by keeping it in an ice bath. To this, 16 eq. of $SnCl_2 \cdot 2H_2O$ in 20 ml of HCl was added and then the reaction mixture was refluxed for 20 h. The reaction mixture was then cooled to room temperature and neutralized with ammonia solution by keeping it at ice bath. The precipitated solid was filtered with a G4 sintered crucible. The solid porphyrin was dissolved in $CHCl_3$ and extracted with 20% NaOH solution. The solvent was evaporated and the crude porphyrin was purified by column chromatography with 85% yield (324 mg, 0.515 mmol).

^{1}H NMR in $CDCl_3$ δ (ppm): 8.9 (d, 2H, *β*-pyrrole), 8.8 (s, 6H, *β*-pyrrole), 8.2 (d, 6H, *meso-o*-phenyl), 7.9 (d, 2H, *meso-m*-phenyl NH_2), 7.7 (m, 9H, *meso-m*, *p*-phenyl), 7.0 (d, 2H, *meso-o*-phenyl NH_2), 4.0 (s, 2H, -NH_2), -2.8 (s, 2H, NH). UV/Vis in CH_2Cl_2: λmax [nm] 420, 516, 553, 592, 646.

RESULTS AND DISCUSSION

Optical Characterization

The absorption and emission spectra of the free base porphyrinic dyes were recorded in CH_2Cl_2 at 298 K (Fig. 1). These dyes exhibit a strong absorption band (Soret band) in the range of 400–440 nm followed by four Q bands in the visible region of 510–655 nm, which can be attributed to π–π* transition of the porphyrin core, which is the characteristic feature of free base porphyrins. Table S1 lists the UV-Vis and fluorescence spectral data of porphyrinic dyes in CH_2Cl_2 at 298 K. No considerable shift was observed in the absorption

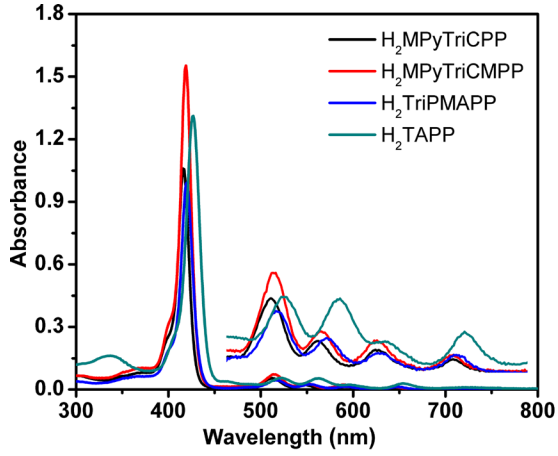

(a)

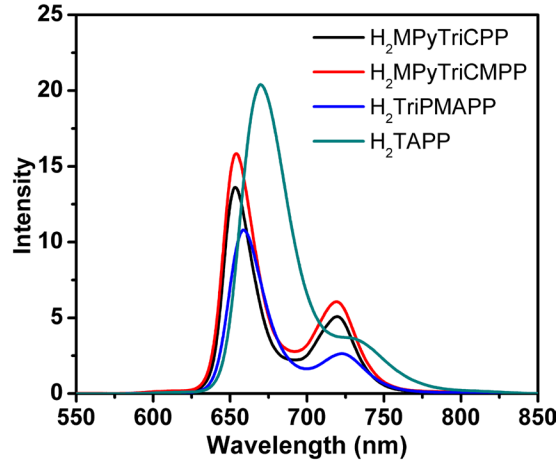

(b)

Fig. 1. (a) The comparative absorption, (b) Emission Spectra of H_2MPyTriCPP, H_2MPyTriCMPP, H_2TriPMAPP and H_2TAPP in CH_2Cl_2 at 298K

wavelength of the porphyrin dyes having carboxylic acid and pyridyl groups, whereas tetra-aminophenylporphyrin (H_2TAPP) exhibited 7–11 nm red shift in the Soret band and 8 nm in $Q_x(0,0)$ band as compared to other dyes due to the presence of four electron donating amino groups which raise the HOMO level resulting in a decrement of the HOMO–LUMO gap.

To elucidate the role of different donor functional groups on the emission profile of the porphyrins, the fluorescence spectra of all synthesized porphyrins were recorded. Figure 1b shows the comparative electronic emission spectra of representative porphyrin dyes in CH_2Cl_2 at 298 K. Porphyrins were excited at B band (in the range of 416–427 nm), and fluorescence was monitored between 575 to 800 nm. The emission spectral data of these porphyrins are listed in Table S1. No significant shift in the emission band was observed for these dyes except in the case of H_2TriPyMCPP and H_2TAPP. These dyes exhibit a marginal red shift of 8–10 nm as compared to other dyes due to the presence of electron-donating groups such as amine and electron-withdrawing pyridyl groups. The electronic absorption and emission spectral data are in good agreement with the reported literature [17–19].

Structural Characterization

Density Functional Theory (DFT) Calculations

The B and Q bands both arise from π–π* transitions and can be explained by a four-molecular orbital model. According to the Gouterman four-orbital model, the absorption band in the porphyrin system arises from transitions between both HOMOs and LUMOs, and it is the identities of the metal center and the substituent on the ring that affect the relative energies of the transitions. For a perfect porphyrin system these orbitals are degenerate due to symmetry of the system which gives two Q states [20]. The substituents attached to the porphyrin core may distort the symmetry while also leading to extended conjugation which strongly influences the frontier orbitals of the porphyrin moiety.

The DFT calculations of these dyes have been carried out using Gaussian 09 with the basis set of 6-31G. The functional (B3LYP) is used due to the reasonable accuracy with affordable computational cost [21]. In all cases, a planar conformation of the porphyrin core has been observed, as shown in Fig. S1. Figure 2 and Figs. S2–S6 show the frontier molecular orbitals of H_2TriPyMCPP and other five porphyrinic dyes used in this study.

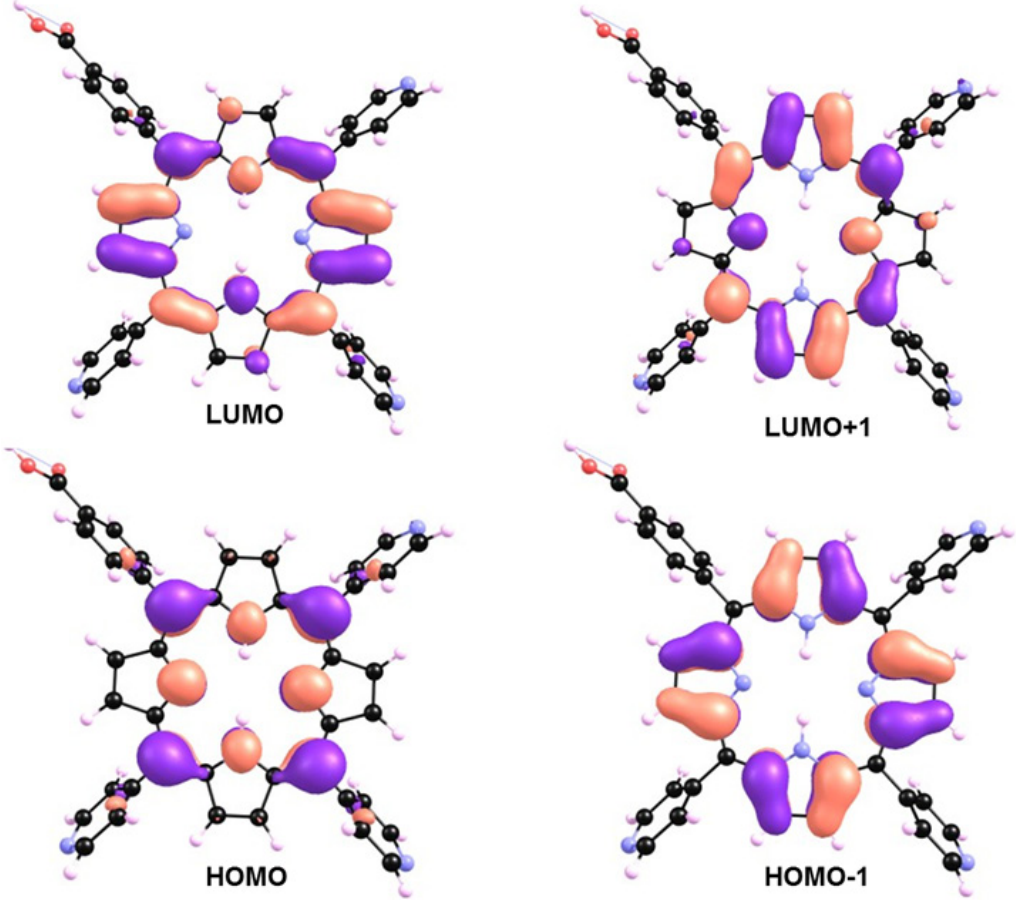

Fig. 2. Frontier molecular orbitals (FMOs) of H_2TriPyMCPP using Gaussian 09 with B3LYP/6-31 G basis sets

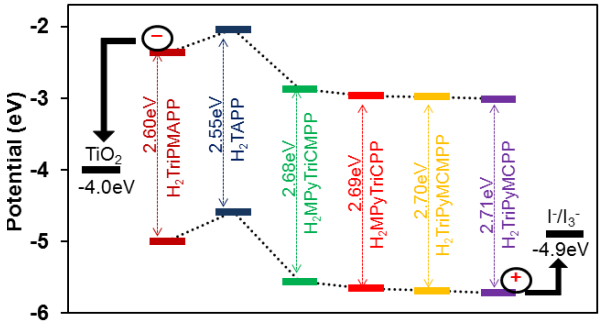

Fig. 3. Energy level diagram of free base porphyrin sensitizers compared with conduction band of nanocrystalline TiO_2 and I^-/I_3^- redox couple

DFT calculations reveal the significant variation of the HOMO and LUMO energy levels in mono/tetra-amino porphyrins as compared to pyridylporphyrins as indicated by the presence of electron density on the phenyl ring of the amino group(s) (Figs. S2 and S3). HOMO–1 of H_2TAPP represents the electronic contribution of amino donor moiety which clearly indicates the possibility of charge transfer from HOMO-1 to LUMO. DFT studies indicate that the major transitions are HOMO to LUMO+1 and HOMO–1 to LUMO.

Figure 3 represents the HOMO–LUMO energy levels of free base porphyrin dyes calculated from DFT studies in comparison with the conduction band of TiO_2 and I^-/I_3^- redox couple indicates the viability of electron transfer. The calculated HOMO energy levels lie in the range of -4.592 to -5.732 eV, while the LUMO energy levels are in the range of -2.041 to -3.017 eV as listed in Table 1. The calculated energy levels are in agreement with transformed CV values [22] as indicated by the data obtained from redox potential and optical energies. The HOMO–LUMO energy gap is lower for amino porphyrins (2.55–2.60 eV from DFT calculation and 2.17–2.20 V from CV studies) as compared to pyridylporphyrins (2.68–2.71 eV from DFT calculations and 2.35–2.37 eV from CV studies) due to the strong electron-donating nature of amino groups. The HOMO and LUMOs are similar in pyridyl porphyrins, whereas the difference in amino porphyrins can be clearly seen in Figure 3. It appears that the electron-donating nature of the $-NH_2$ group causes a higher shift in the HOMO energy level of H_2TAPP as compared to H_2TriPMAPP as shown in Table 1. The distribution of HOMO–LUMO energy levels in porphyrinic dyes is largely localized in donor and acceptor groups [23]. The conduction band of TiO_2 is located at -4.0 eV, while the redox potential of the electrolyte is located at -4.9 eV as shown in Fig. 3 [1, 4a]. These porphyrins are sufficient to ascertain the injection and regeneration reaction from a thermodynamic point of view. Figure 3 clearly indicates the feasibility of electron transfer from porphyrin to the CB of TiO_2.

SEM images of a bare, sintered TiO_2 layer and the porphyrin dye loaded TiO_2 layer are shown in Figs 4a and 4b, respectively. Highly porous electrode layers with large surface areas are readily available to dyes for rapid adsorption, thus enhancing the short circuit current density. As a result, mesoporous electrode materials show enhanced electrochemical performance compared with their bulk counterparts [24]. The presence of holes and extensive bridging as depicted in Fig. 4a is an indicator of highly conducting mesoporous and crystalline TiO_2 layers whereas Fig. 4b reveals extensive adsorption of the porphyrin dye on the TiO_2 nanoparticles.

Photovoltaic studies

The DSSCs were sensitized using synthesized free base porphyrin dyes on mesoporous nanocrystalline TiO_2 photoanodes assembled into standard sealed sandwiched cells with Pt sheet counter electrode and iodide/triiodide electrolyte. Figure 5 shows the I–V characteristics of the DSSC using various free base porphyrins. Table 2 lists the photovoltaic parameters of free base porphyrinic dyes. We have obtained the photon-to-current conversion efficiency (PCE%) in the range of 0.0039% to 3.26%. The DSSCs sensitized with H_2TriPyMCPP have shown the highest conversion efficiency of 3.26%, possibly due to the presence of a higher number of pyridyl groups acting as electron injecting anchoring groups. It is reported that the pyridyl ring present in the dye enables good electronic communication between the dye and TiO_2 due to the formation of a coordinate bond between the pyridine ring of the dye and the Lewis acid site of the TiO_2 surface [25].

Table 1. Calculated energy levels and HOMO–LUMO gap in (eV) obtained from DFT calculations

Porphyrins	HOMO-1 (ev)	HOMO (ev)	LUMO (ev)	LUMO+1 (ev)	HOMO–LUMOgap (ev)
H_2TriPMAPP	-5.425	-4.999	-2.367	-2.331	2.60
H_2TAPP	-5.106	-4.592	-2.041	-2.004	2.55
H_2MPyTriCMPP	-5.913	-5.563	-2.875	-2.857	2.68
H_2MPyTriCPP	-6.003	-5.658	-2.969	-2.915	2.69
H_2TriPyMCMPP	-6.025	-5.690	-2.984	-2.963	2.70
H_2TriPyMCPP	-6.056	-5.723	-3.017	-2.996	2.71

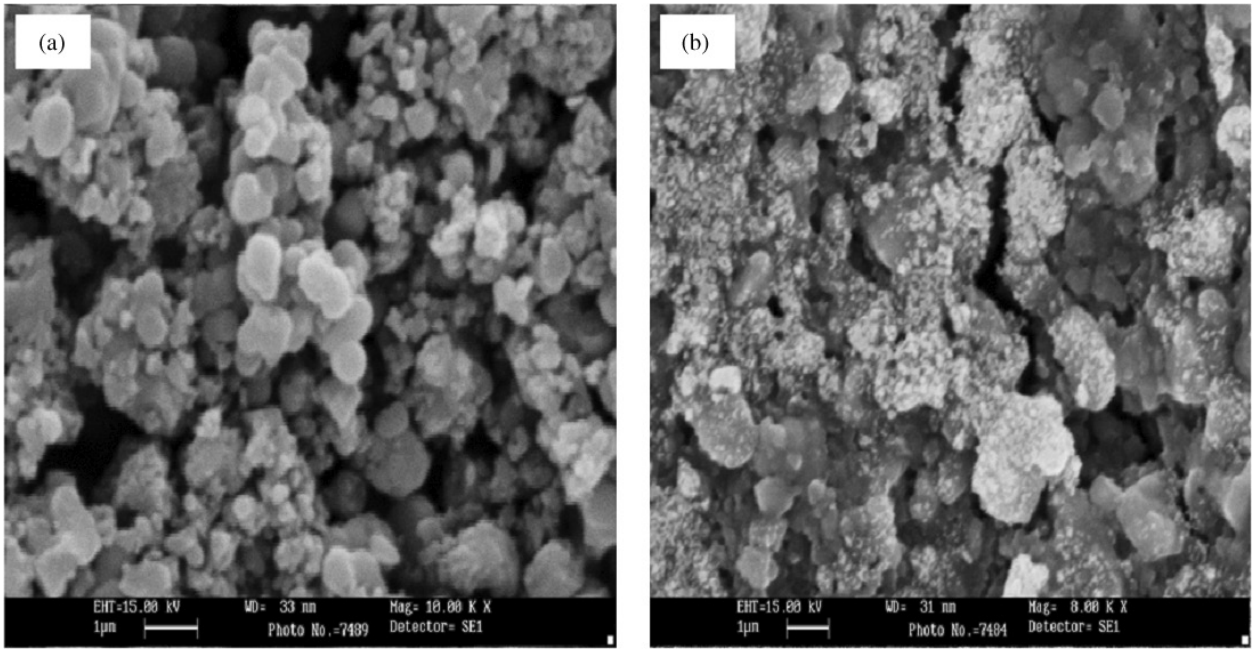

Fig. 4. SEM images of (a) bare TiO_2 layer and (b) porphyrin dye loaded TiO_2 layer

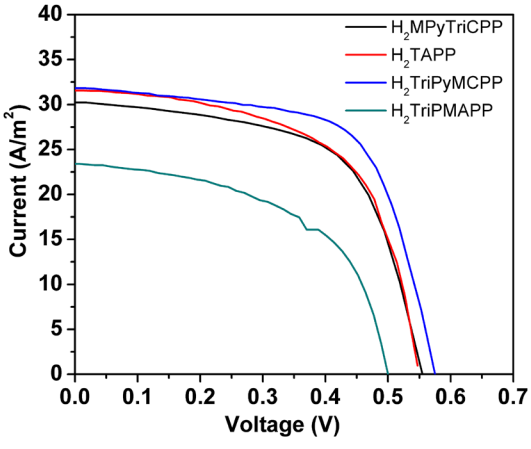

Fig. 5. The typical I–V curve under 350 W/m^2 solar illumination for the DSSC using synthesized free base porphyrin dyes

H_2TAPP achieved the second highest performance in power conversion efficiency among the dyes tested, due to the presence of more number of electron donating anchoring groups. In agreement with this H_2TAPP with four anchoring -NH_2 groups shows approximately four times higher efficiency as compared to H_2TriPMAPP having one anchoring -NH_2 group. The dyes with ester groups have shown negligible PCE% values as compared to their counterpart dyes having acid groups, as they cannot coordinate with TiO_2 effectively, unlike -COOH.

The power conversion efficiency (η) of the above reported free base dyes follows the order: H_2TriPyMCMPP (η = 0.0083%) < H_2MPyTriCMPP (η = 0.0093%) < H_2TriPMAPP (η = 0.7%) < H_2MPyTriCPP (η = 2.84%) < H_2TAPP (η = 2.94%) H_2TriPyMCPP (η = 3.26%).

The incident photon to current efficiency (IPCE) spectra were measured and was performed as a function of incident wavelength to evaluate the photovoltaic performance. The IPCE spectra of fabricated solar cells are shown in Fig. S7 in the Supporting information. In all cases, the solar cells fabricated using H_2TriPyMCPP exhibited good IPCE response in Soret band region, which is consistent with a higher Jsc value (Table 2) as compared to other dyes. The amino porphyrin dyes

Table 2 Photovoltaic parameters of free base porphyrins under 350 W/m^2 solar illumination with an active area of 0.15 cm^2

Porphyrin	V_{oc} (V)	J_{sc} (A/m^2)	Fill factor	Efficiency (η)
H_2MPyTriCPP	0.555	30.00	0.610	2.84%
H_2MPyTriCMPP	0.233	0.38	0.370	0.00934%
H_2TAPP	0.547	31.67	0.595	2.94%
H_2TriPyMCPP	0.575	31.82	0.642	3.26%
H_2TriPyMCMPP	0.233	0.15	0.378	0.00385%
H_2TriPMAPP	0.502	23.44	0.545	0.7%

demonstrated moderate response while the ester group containing porpyrinic dyes exhibited very poor response towards IPCE, which is consistent with the Jsc and Voc values.

H_2TriPyMCPP showed Voc, Jsc and fill factor values of 575 mV, 31.82 A/m2 and 0.642, respectively with the PCE value of (η) 3.26% (Table 2).

CONCLUSIONS

In summary, we have synthesized *meso*-substituted A_3B/A_4 free base porphyrins having pyridyl, carboxy phenyl and amino groups in good yields *via* a simplified two-step process, and we have investigated the effect of these functional groups on their photosensitization properties. The highest power conversion efficiencies (η) of 3.26%, 2.94% and 2.84% were achieved for the DSSC fabricated using H_2TriPyMCPP, H_2TAPP and H_2MPyTriCPP dyes, respectively. The introduction of more number of electron donating groups such as the $–NH_2$ group enhances the PCE% as depicted by H_2TAPP which shows a fourfold higher efficiency (2.84%) as compared to H_2TriPMAPP (0.7%). Tripyridyl monocarboxyphenylporphyrin has shown higher PCE value as compared to monopyridyltricarboxyphenylporphyrin due to efficient coordination and feasible electron injection from pyridyl group(s) to TiO_2. Porphyrins having more numbers of electron-donating/electron-injecting groups as well as anchoring amino/pyridyl groups show higher power conversion efficiency as compared to porphyrins with lower number of pyridyl/amino groups.

Acknowledgments

We sincerely thank Science and Engineering Research Board (SB/FT/CS-015/2012) and Board of Research in Nuclear Science (2012/37C/61/BRNS) for financial support. NC thanks CSIR, India for senior research fellowship.

REFERENCES

1. (a) O'Regan B and Grätzel M. *Nature* 1991; **353**: 737–740. (b) Grätzel M. *Nature* 2001; **414**: 338–344. (c) Hagfeldt A, Boschloo G, Sun L, Kloo L and Pettersson H. *Chem. Rev.* 2010; **110**: 6595–6663.
2. (a) Grätzel M. *Acc. Chem. Res.* 2009; **42**: 1788–1798. (b) Clifford JN, Martinez-Ferrero E, Viterisi A and Palomares E. *Chem. Soc. Rev*. 2011; **40**: 1635–1646.
3. (a) Hardin BE, Snaith HJ and McGehee MD. *Nat. Photonics* 2012; **6**: 162–169. (b) Satapathi S, Gill HS, Li L, Samuelson L, Kumar J and Mosurkal R. *Appl. Surf. Sci*. 2014; **323**: 13–18.
4. (a) Nazeeruddin MK, Angelis FD, Fantacci S, Selloni A, Viscardi G, Liska P, Ito S, Takeru B and Grätzel M. *J. Am. Chem. Soc.* 2005; **127**: 16835–16847. (b) Yu Y, Wang Z, Yi N, Zu J, Zhang M and Wang P. *ACS Nano* 2010; **4**: 6032–6038. (c) Spettel KE and Damrauer NH. *J. Phys. Chem. C* 2016; **120**: 10815–10829.
5. Chen CY, Wang M, Li JY, Pootrakulchote N, Alibabaei L, Ngoc-Le CH, Decoppet JD, Tsai JH, Grätzel G, Wu CG, Zakeeruddin SM and Grätzel M. *ACS Nano* 2009; **3**: 3103–3109.
6. Giribabu L and Kanaparthi RK. *Curr. Sci.* 2013; **104**: 847–855.
7. Han L, Islam A, Chen H, Malapaka C, Chiranjeevi B, Zhang S, Fang X and Yanagida M. *Energy Environ. Sci.* 2012; **5**: 6057–6060.
8. (a) Ito S, Zakeeruddin SM, Humphry-Baker R, Liska P, Charvet R, Comte P, Nazeeruddin MK, Pechy P, Takata M, Miura H, Uchida S and Grätzel M. *Adv. Mater*. 2006; **18**: 1202–1205. (b) Shibano Y, Umeyama T, Matano Y and Imahori H. *Org. Lett*. 2007; **9**: 1971–1974. (c) Wang ZS, Cui Y, Dan-Oh Y, Kasada C, Shinpo A and Hara K. *J. Phy. Chem. C* 2008; **112**: 17011–17017.
9. (a) Ushiroda S, Ruzycki N, Lu Y, Spitler MT and Parkinson BA. *J. Am. Chem. Soc*. 2005; **127**: 5158–5168. (b) Jung I, Lee JK, Song KH, Song K, Kang SO and Ko J. *J. Org. Chem*. 2007; **72**: 3652–3658. (c) Kakiage K, Aoyama Y, Yano T, Oya K, Fujisawa JI and Hanaya M. *Chem. Commun*. 2015; **51**: 6315–6317.
10. Campbell WM, Burrell AK, Officer DL and Jolley KW. *Coord. Chem. Rev*. 2004; **248**: 1363–1379. (b) Ball JM, Davis NKS, Wilkinson JD, Kirkpatrick J, Teuscher J, Gunning R, Anderson HL and Snaith HJ. *RSC Adv*. 2012; **2**: 6846–6853 (c) Lodermeyer F, Costa RD, Malig J, Jux N and Guldi GM. *Chem.-Eur. J*. 2016; **22**: 7851–7855. (c) Kumar R, Sankar M, Sudhakar V and Krishnamurthy K. *New J. Chem*. 2016; **40**: 5704–5713.
11. (a) Mathew S, Yella A, Gao P, Humphry-Baker R, Curchod FEB, Ashari-Astani N, Tavernelli I, Rothlisberger U, Nazeeruddin MK and Grätzel M. *Nature Chem*. 2014; **6**: 242–247. (b) Yella A, Lee HW, Tsao HN, Yi C, Chandiran AK, Nazeeruddin MK, Diau EWG, Yeh CY, Zakeeruddin SM and Grätzel M. *Science* 2011; **334**: 629–634 (c) Magnano G, Marinotto D, Cipolla MP, Trifiletti V, Listorti A, Mussini PR, Di. Carlo G, Tessore F, Manca M, Biroli AO and Pizzotti M. *Phys. Chem. Chem. Phys*. 2016; **18**: 9577–9585.
12. (a) Nazeeruddin MK, Humphry-Baker R, Officer DL, Campbell WM, Burrel AK and Grätzel M. *Langmuir*, 2004; **20**: 6514–6517. (b) Wang Q, Campbell WM, Bonfantani EE, Jolley KW, Officer DL, Walsh PJ, Gordon K, Humphry-Baker R, Nazeeruddin MK and Grätzel M. *J. Phys. Chem. B* 2005; **109**: 15397–15409. (c) Lee CW, Lu HP, Lan CM, Huang YL, Liang YR, Yen WN, Liu YC, Lin

YS, Diau EW and Yeh CY. *Chem.-Eur. J.* 2009; **15**: 1403–1412.
13. (a) Schmidt-Mende L, Campbell WM, Wang Q, Jolley KW, Officer DL, Nazeeruddin MK and Grätzel M. *Chem. Phys. Chem*. 2005; **6**: 1253–1258.
14. Ma R, Guo P, Cui H, Zhang X, Nazeeruddin MK and Grätzel M. *J. Phys. Chem. A* 2009; **113**: 10119–10124. (b) Urbani M, Grätzel M, Nazeeruddin MK and Torres T. *Chem. Rev*. 2014; **114**: 12330–12396.
15. Tayade RJ, Kulkarni RG and Jasra RV. *J. Ind. Eng. Chem*. 2006; **45**: 922–927.
16. Kim SH and Park CW. *Bull. Korean Chem. Soc*. 2013; **34**: 831–836.
17. Habdas J and Boduszek B. *J. Pept. Sci.* 2009; **15**: 305–311.
18. Sankar M, Liptsman S and Goldberg I. *Acta. Cryst.* 2007; **63**: 395–399.
19. Bettelheium A, White BA, Raybuck SA and Murray RW. *Inorg. Chem.* 1986; **26**: 1009–1017.
20. Gouterman M. *J. Mol. Spectrosc*. 1961; **6**: 138–163.
21. (a) Pastore M, Fantacci S and De Angelis F. *J. Phys. Chem. C* 2010; **114**: 22742–22750. (b) Meng S, Kaxiras E, Nazeeruddin MK and Grätzel M. *J. Phys. Chem. C* 2011; **115**: 9276–9282.
22. Magnano G, Marinotto D, Cipolla MP, Trifiletti V, Listorti A, Mussini PR, Di Carlo G, Tessore F, Manca M, Biroli AO and Pizzotti M. *Phys. Chem. Chem. Phys*. 2016; **18**: 9577–9585.
23. Wei T, Sun X, Li X, Ågren H and Xie Y. *ACS Appl. Mater. Interfaces* 2015; **7**: 21956–21965.
24. Guo YG, Hu JS and Wan LJ. *Adv. Mater*. 2008; **20**: 2878–2887.
25. (a) Ooyama Y, Nagano T, Inoue S, Imae I, Komaguchi K, Ohshita J amd Harima Y. *Chem.-Eur. J.* 2011; **17**: 14837-14843.(b) Daphnomili D, Landrou G, Sing SP, Thomas A, Yesudas K, Bhanuprakash K, Sharma GD, Coutsolelos AG. *RSC Adv*. 2012; **2**: 12899–12908.